Small-Angle X-Ray Scattering from Polyethylene: Distorted Lamellar Structures

Carla Marega, Antonio Marigo, Valerio Causin

Dipartimento di Chimica Inorganica, Metallorganica ed Analitica dell'Università via Loredan, 4, 35131 Padova, Italy

Received 19 December 2002; accepted 28 February 2003

ABSTRACT: Some theoretical models, including lamellar distortions of the second kind, are described. To test the influence of lamellar distortions on the small-angle X-ray scattering (SAXS) of polymers, some theoretical patterns were calculated with different values of the model parameters. SAXS diffraction profiles were recorded for three commercial copolymer samples of linear low-density polyethylene containing different comonomers and one commercial homopolymer sample of high-density polyethylene; these were successively analyzed by a fit to the calculated profiles corresponding to our theoretical models. Transmission electron microscopy images were obtained of the lamellar morphologies of the four samples. From these, we concluded that the homopolymer sample displayed excellent organization on lamellar stacks, whereas the copolymer samples showed more imperfect lamellar morphologies, so it was useful, in the latter case, to introduce a distorted lamellar structure in calculated SAXS diffraction patterns. By use of wide-angle X-ray scattering, we also determined the overall crystallinities of the samples. © 2003 Wiley Periodicals, Inc. J Appl Polym Sci 90: 2400–2407, 2003

Key words: polyethylene (PE); SAXS; lamellar; morphology; modeling

INTRODUCTION

The small-angle X-ray scattering (SAXS) technique can play a major role in the structural characterization of multilayers and is often applied in the field of polymer science.

The lamellar structures of semicrystalline polymers are multilayers whose structures are represented by two kinds of layers alternately stacked (crystalline lamellae and amorphous regions).

Many theoretical models have been described in the literature[1,2] and applied to many polymers.[3,4]

In most of these theoretical models, lamellar stacking is assumed to have an infinite lateral width; as a consequence, a one-dimensional variation is considered for the electron density. Moreover, a discrete number of lamellae (N) is often introduced to improve the fitting between the experimental and the calculated SAXS patterns.

The method in general leads to a good agreement; however, sometimes the N present in the stacks must be reduced to 1 or 2. It is often useful to modify these models by a consideration of some kind and amount of distortion within the lamellar stacks.

In this study, we considered lamellar distortions of the second kind,[5] which preserve only the short-range order. We applied such a model to four commercial samples of polyethylene: one high-density polyethylene (HDPE) homopolymer and three linear low-density polyethylene (LLDPE) copolymers.

To support our considerations, we also used transmission electron microscopy (TEM) and wide-angle X-ray scattering (WAXS). These techniques allowed us to obtain images of the lamellar structures and to calculate the overall crystallinities (Φ) of the samples.

THEORETICAL CONSIDERATIONS

The effects on the SAXS patterns of second-kind distortions can be explained on the basis of the Vonk's formula:[5]

$$\gamma_1(x) = \gamma_1^0(x)\,\exp(-2x/d) \tag{1}$$

where $\gamma_1(x)$ is the one-dimensional correlation function and $\gamma_1^0(x)$ is the one for ideal lamellar structures, x is the distance perpendicular to the lamellar surface, and d is the distortion length:[5] the value of d increases with decreasing bending of the lamellae.

According to the Wiener–Khintchine theorem,[6] the one-dimensional SAXS intensity function [$I_1(s)$, where $s = 2\sin\theta/\lambda$, 2θ is the diffraction angle and λ is the radiation wavelength] is given as the Fourier cosine transform of the $\gamma_1(x)$ function:

$$I_1(s) = F_c[\gamma_1^0(x)\,\exp(-2x/d)] = F_c[\gamma_1^0(x)]^* F_c[\exp(-2x/d)] \tag{2}$$

Correspondence to: C. Marega (carla.marega@unipd.it).

Journal of Applied Polymer Science, Vol. 90, 2400–2407 (2003)

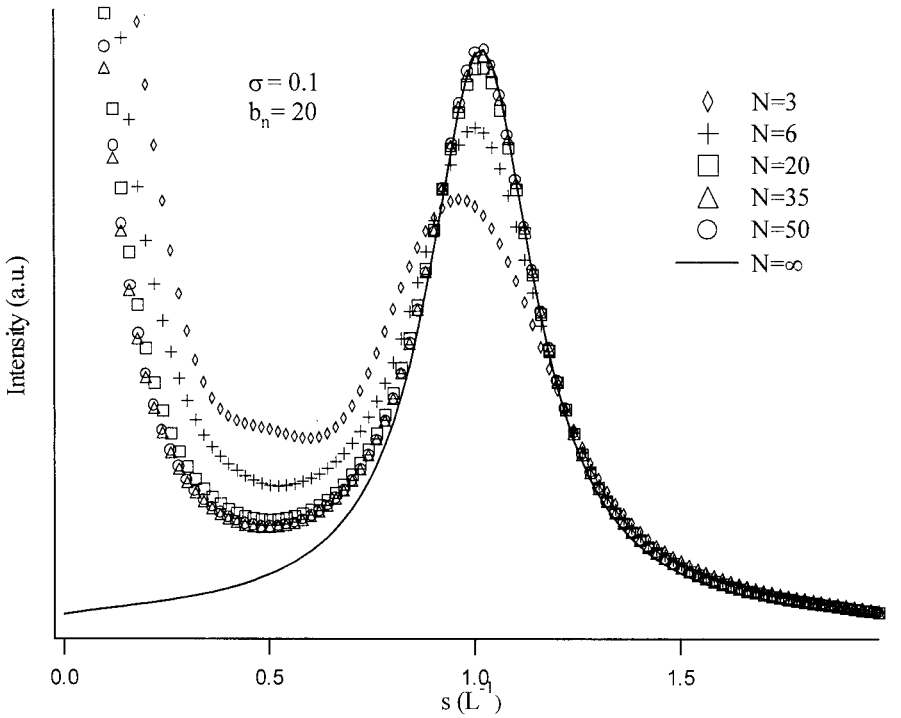

Figure 1 Calculated SAXS intensity curves corresponding to different N values at $\sigma = 0.1$ and $b_n = 20$.

where $F_c[\ ]$ and the asterisk denote the Fourier cosine and the convolution respectively, so

$$I_1(s) = I_1^0(s) * \left[\frac{2/d}{s^2 + (2/d)^2}\right] \tag{3}$$

where $I_1^0(s)$ is the one-dimensional SAXS intensity function for ideal lamellar structure.[2]

If $d \to \infty$, $\left[\frac{2/d}{s^2 + (2/d)^2}\right] \to \delta(s)$ [where $\delta(s)$ denotes the Dirac's delta function], and $I_1(s)$ reduces to $I_1^0(s)$.

Models

The four models described in ref. 2, and which are addressed here, could be improved by the application of eq. (3), which considers the distortions of the second kind.

Simple lamellar stack model

The first model is based on a single lamellar stacking, which represents, according to a statistical formulation, the whole sample. Furthermore, it assumes that N is so large that it can be considered infinite. In the second model, a discrete N is introduced, which broadens the SAXS peaks because of finite lattice size.[1]

Variable lamellar stack model

A third model was considered, where an infinite N is introduced; however, it is assumed that there is a longer range inhomogeneity than in the single stack model, in which there are Φ fluctuations among the stacks and within each stack as well.

For this model, the intensity can no longer be represented by a single statistical stack but is the average of the whole stack distribution.

Finally, the last (fourth) model is a modification of the third by the introduction into the calculation of a finite N.

Theoretical calculations

To test the influence of lamellar distortions on the SAXS spectra, we first calculated some theoretical SAXS profiles corresponding to different values of N, σ_C [standard deviation of the average crystal thickness (C)], and the distortion parameter (b_n; $d = b_n D$, where D is the long period).

We evaluated the theoretical intensity profiles by putting $D = 1.0$ on a length scale (L), and we set C to $0.5L$. Furthermore, for simplicity, $\sigma = \sigma_A = \sigma_C$ [where σ_A is the standard deviation of the amorphous thickness (A)].

Figure 1 shows the calculated SAXS intensity curves corresponding to different N values at $\sigma = 0.1$ and $b_n = 20$. The decrease in N tended to cause a lower

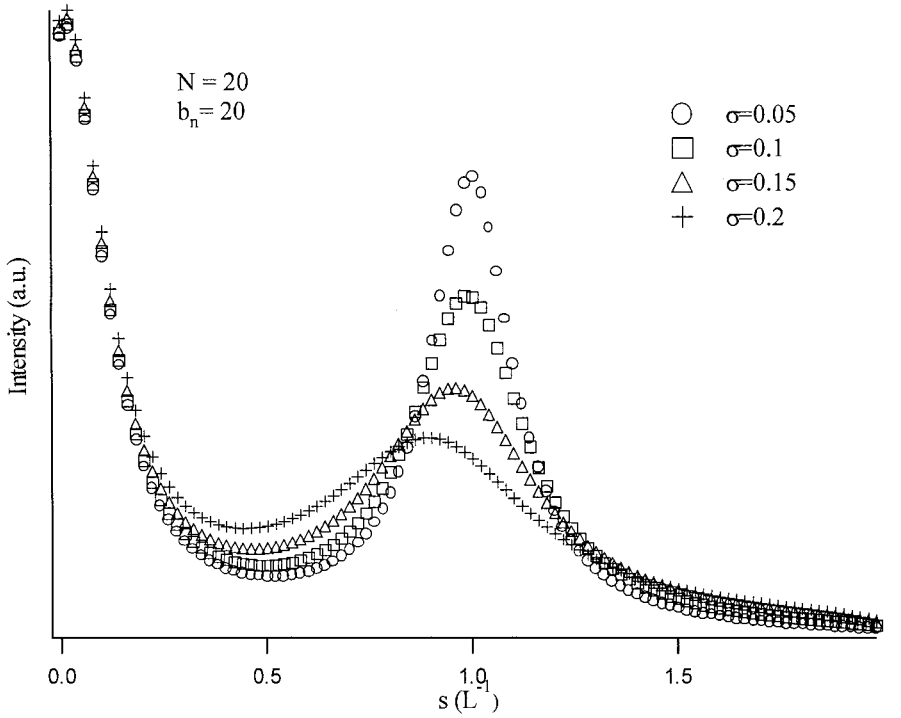

Figure 2 Calculated SAXS intensity curves corresponding to different σ values at $N = 20$ and $b_n = 20$.

intensity and broader first-order maximum. It also promoted an increase of the zero-order maximum when N changed from ∞ to a finite value.

Figure 2 shows the effects on the calculated SAXS profiles of different σ values at $N = 20$ and $b_n = 20$. A decrease and broadening of the first-order maximum occurred, whereas the zero-order maximum was unchanged.

Figure 3 shows the behavior of the calculated SAXS profiles when b_n decreased at $N = 20$ and $\sigma = 0.2$.

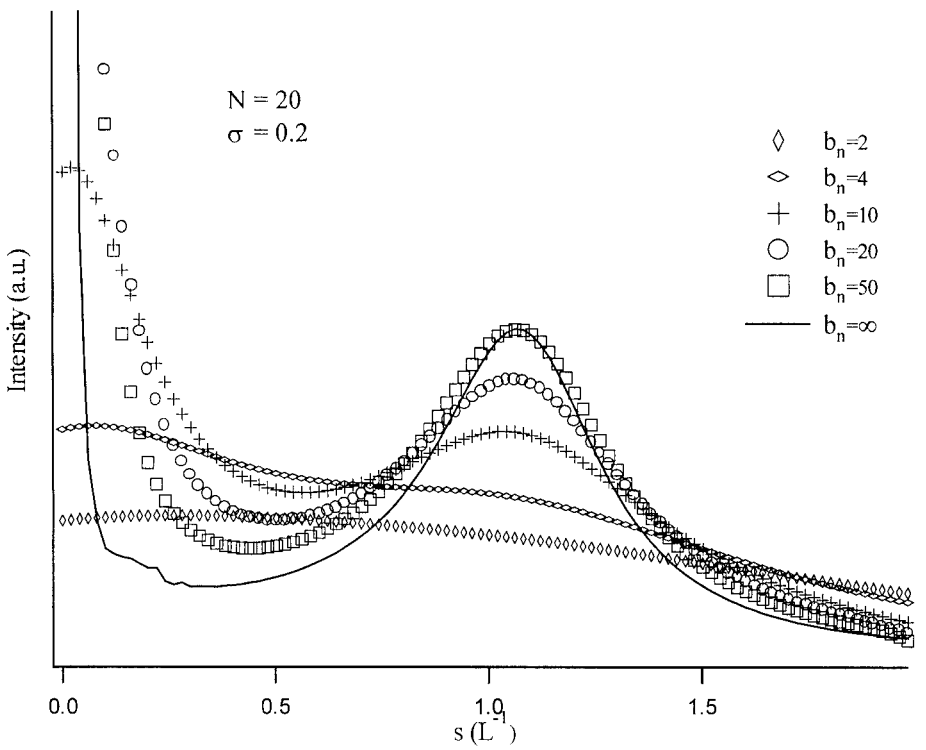

Figure 3 Calculated SAXS intensity curves corresponding to different b_n values at $N = 20$ and $\sigma = 0.2$.

TABLE I
Characterization of HDPE and LLDPE Samples: Comonomer, Comonomer Content, [η], $\overline{M}_n$,$\overline{M}_w$, Molecular Weight Distribution ($\overline{M}_w/\overline{M}_n$), and Density

Sample	Comonomer	Comonomer content (mol %)	[η]	$\overline{M}_n$	$\overline{M}_w$	$\overline{M}_w/\overline{M}_n$	Density (g/cm^3)
HEX	1-hexene	5.0	1.48	18500	94500	5.1	0.9192
PEN	4-me-1-pentene	3.8	2.59	29100	213000	7.3	0.9227
BUT	1-butene	4.5	1.80	23100	130000	5.6	0.9253
HOM	—	—	0.98	16300	57000	3.5	0.9656

Here, we observed a decrease of the first-order and of the zero-order maxima as well.

The three figures were the choice of a large number of tests we did to study the influence on the calculated SAXS patterns of the changes of the parameters N, σ, and b_n.

EXPERIMENTAL

The one-homopolymer sample of HDPE (HOM) and three samples of LLDPE[7] containing different comonomers [1-butene (BUT), 4-methyl-1-pentene (PEN), and 1-hexene (HEX)] were analyzed, and the comonomer contents (mol %) are reported in Table I.

The original pellets of the four commercial samples were transformed into plates by compression-molding for 10 min at 150°C (LLDPE) or 180°C (HDPE) and were then slowly cooled into the press for 6 h to room temperature. The plates were 2.5 mm thick.

The number-average molecular weights ($\overline{M}_n$'s) and weight-average molecular weights ($\overline{M}_w$'s) of the HDPE and LLDPE samples were evaluated by gel permeation chromatography in a Spherosil column (Paris, France) (103–107 Å) at 135°C with 1,2-dichlorobenzene (LLDPE) or 1,2,4-trichlorobenzene (HDPE) as an eluent. These data are reported in Table I, together with comonomer content (LLDPE), intrinsic viscosity ([η]), and density data.

TEM

Specimens for TEM observations were first stained with RuO4; then, they were sectioned in a Reichert Ultracut S ultramicrotome (Depew, NY), equipped with a cryogenic device for cutting at low temperatures (specimen = −140°C, knife = −60°C). The ultrathin slices were placed on copper grids and observed in a Philips 301 electron microscope (Almelo, The Netherlands) at 80 kV.

The images obtained by TEM allowed us to see the lamellar morphologies of the samples and the regularity of the organization on stacks; therefore, it was possible to prove the presence of lamellar distortions on some of the samples and to correlate it to the SAXS calculations.

WAXS

The WAXS patterns of the samples were recorded in the diffraction angular range $2\theta = 10$–$50°$ with a transmission diffractometer GD2000 (Riva del Garda, Italy) working with Seemann–Bohlin geometry and a quartz crystal monochromator of the Johansson type on the primary X-ray beam. Cu Kα_1 radiation was used.

The application of the least-squares fit procedure elaborated by Hindeleh and Johnson[8] gave the degree of crystallinities determined by WAXS (Φ_{WAXS}'s) and reported in Table II.

SAXS

The SAXS measurements were performed in a MBraun system with Cu Kα radiation from a Philips PW1830 X-ray generator (Garching, Germany). The patterns were recorded by a position-sensitive detector in the scattering angular range $2\theta = 0.1$–$5.0°$ and corrected for the blank scattering. A constant continuous background scattering[9] was subtracted, and the obtained intensity values [$\tilde{I}(s)$'s] were smoothed in the tail region with the aid of the $s\tilde{I}(s)$ versus $1/s^2$ plot.[10] Then, Vonk's desmearing procedure[11] was applied, and $I_1(s)$ was obtained with the Lorentz correction: $I_1(s) = 4\pi s^2 I(s)$, where $I_1(s)$ is the one-dimensional scattering function and $I(s)$ is the desmeared intensity function.

The sum of C and A was determined as the Bragg identity period (D) of $I_1(s)$.

Calculation procedure

The evaluation of the SAXS intensity corresponding to the considered models was carried out by the use of

TABLE II
Φ of HDPE and LLDPE Samples

Sample	$\Phi(\%)_{WAXS}$	$\Phi(\%)_{SAXS}$
HEX	42	32
PEN	52	36
BUT	41	33
HOM	73	81

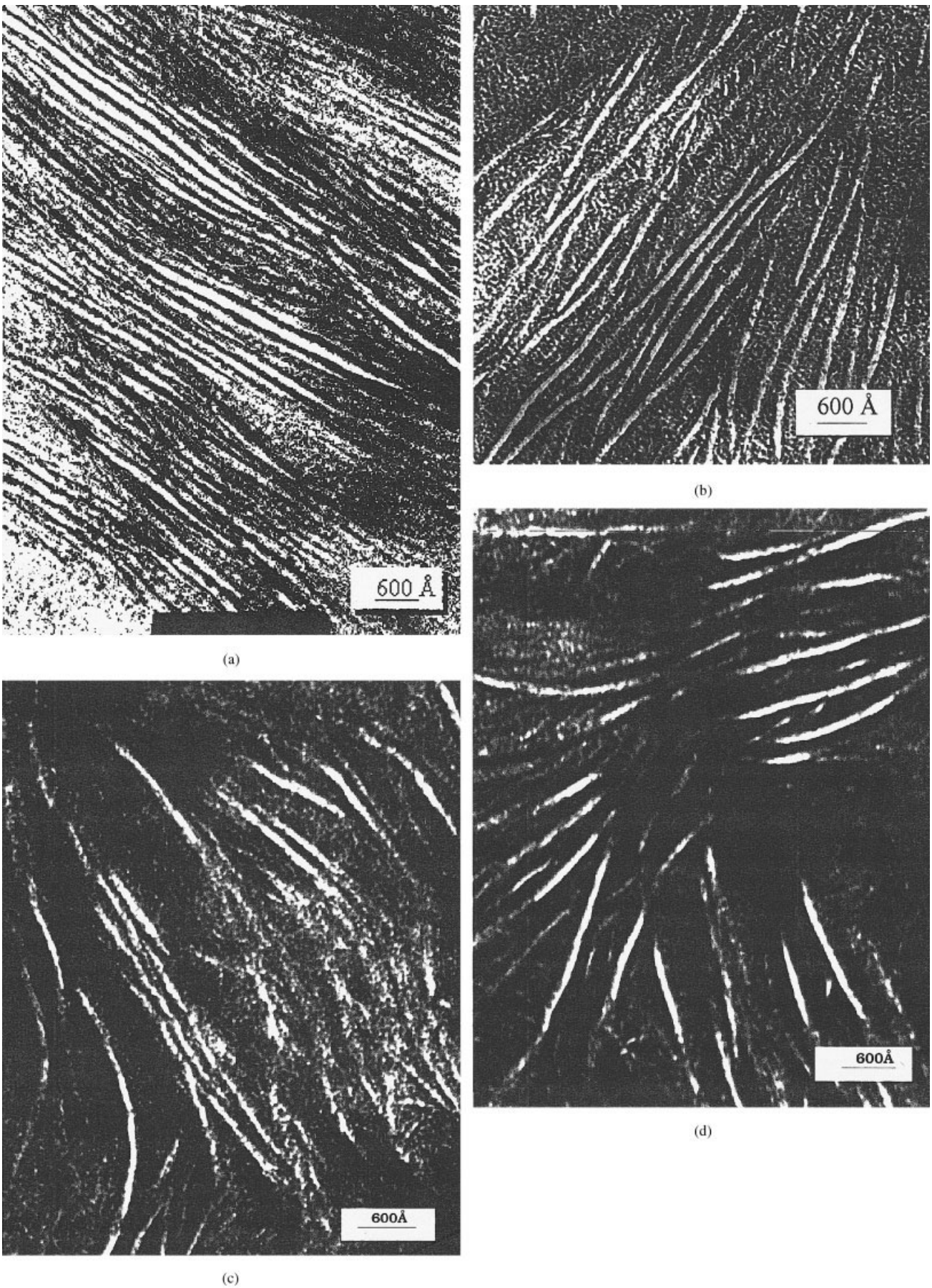

Figure 4 TEM images of the (a) HOM, (b) HEX, (c) PEN, and (d) BUT samples.

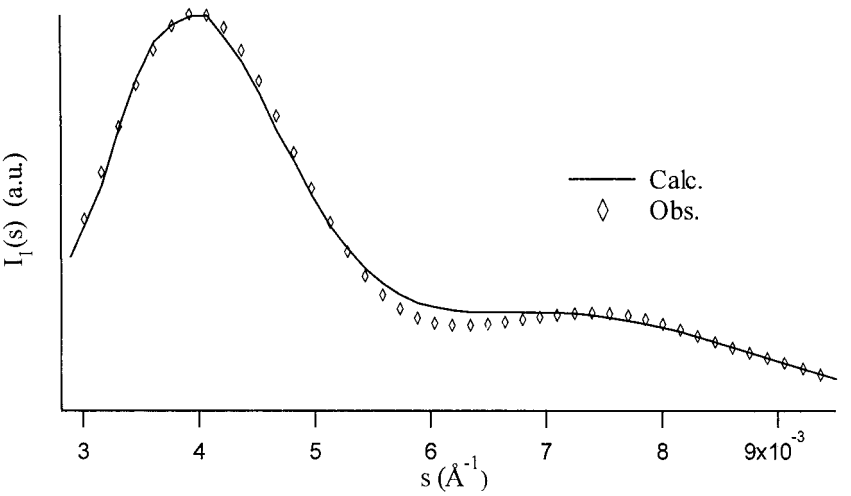

Figure 5 Best fit between the experimental and calculated SAXS patterns obtained for the HOM sample.

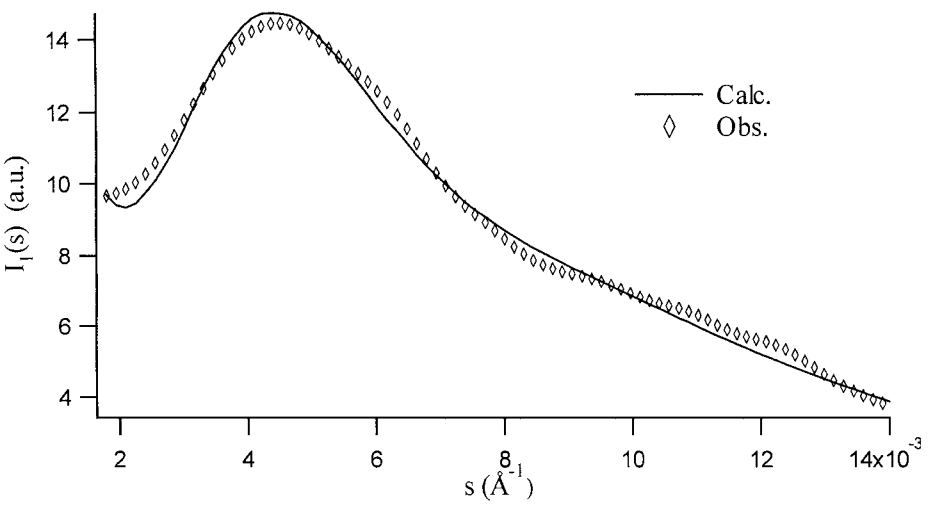

Figure 6 Best fit between the experimental and calculated SAXS patterns obtained for the HEX sample.

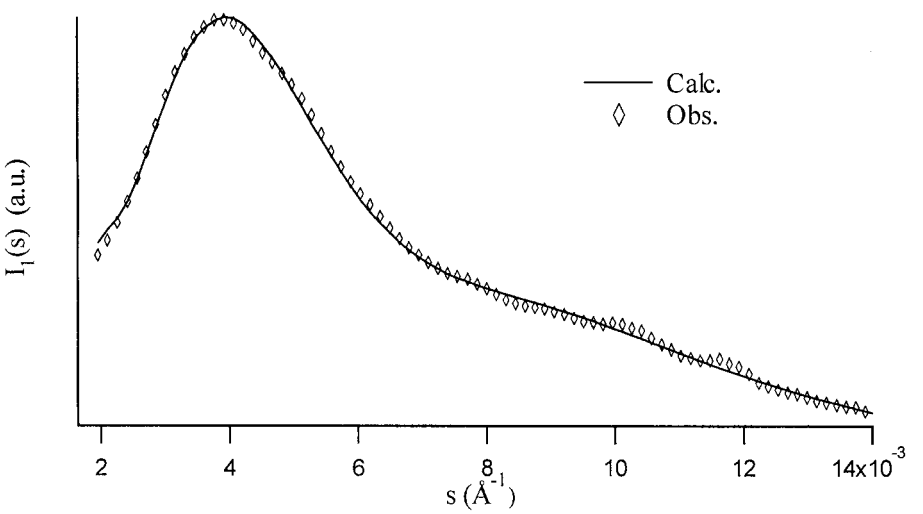

Figure 7 Best fit between the experimental and calculated SAXS patterns obtained for the PEN sample.

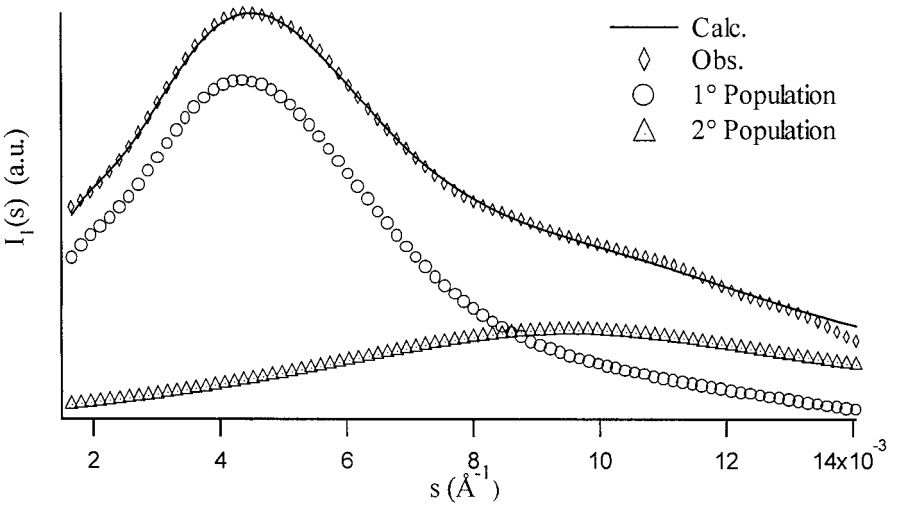

Figure 8 Best fit between the experimental and calculated SAXS patterns obtained for the BUT sample.

eq. (3). The simulation algorithm was linked to the MINUIT least-square procedure[12] to allow an evaluation of the main structural parameters. The goodness of each fit was given by R_{WP}, which accounted[13] for the weighted differences between the observed and calculated profiles. The parameters were optimized by a fit between the experimental and calculated SAXS patterns.

For the simple lamellar stack model, the optimized parameters were as follows:

1. N.
2. C.
3. Φ.
4. σ_C.
5. b_n.

The A and σ_A values were evaluated as in ref. 2.

In the case of the variable lamellar stack model, the optimized parameters were as follows:

1. N.
2. Φ.
3. The standard deviation with reference to crystallinity (σ_Φ).
4. A.
5. σ_C.
6. b_n.

RESULTS AND DISCUSSION

The examined models were applied to the polyethylene samples to evaluate when and how the distortions affected the SAXS patterns.

To evaluate the validity of the applied model, we investigated the samples by TEM to have an immediate view of the morphology of the lamellar structure and of the regularity of stacks organization.

Figure 4(a–d) shows a selection of TEM images of the samples.

It was evident that the HOM sample [Fig. 4(a)] presented an excellent organization on stacks, and it showed more extended lamellae, which appeared regular and straight. A good organization in lamellar stacks was also present in the HEX sample [Fig. 4(b)], but a rather distorted lamellar structure, with more curved and shorter lamellae, was evident for the PEN and BUT samples [Figs. 4(c,d)], even though the lamellae of the PEN sample were thicker than the ones of the BUT sample.

The best fits obtained, which applied to the theoretical model previously described, are shown on Figures 5–8.

For the HOM sample (Fig. 5), the best fit (R_{WP} = 2.75%) was obtained with the variable lamellar stack model without distortions; only a single population of lamellar stacks was considered and $N = \infty$. The fit parameters are reported in Table III.

We applied the distortion model to calculate the SAXS profiles for this sample to check if the introduction of lamellar distortions could have improved the fit between the experimental and the calculated spectra. Actually, the value obtained for b_n was ∞, corresponding to $d = \infty$, that is [see eq. (3)], to a situation of regular lamellar stacks.

Figure 6 shows the best fit obtained for the HEX sample (R_{WP} = 2.6%); here, we used the simple lamellar stack model with distortions and two populations,

TABLE III
Fit Parameters for the HOM Sample: D, C, A, Standard Deviation of D σ_D, σ_C, σ_A, Φ, and σ_Φ, and N

Sample	D (Å)	C (Å)	A (Å)	σ_D	σ_C	σ_A	Φ	σ_Φ	N
HOM	265	216	49	0.14	0.17	0.16	81	0.044	∞

TABLE IV
Best Fit Parameters for the HEX, PEN, and BUT Samples; D, C, A, σ_D σ_C, σ_A, Φ, N, and b_n

Sample	D_1 (Å)	C_1 (Å)	A_1 (Å)	σ_{D1}	σ_{C1}	σ_{A1}	D_2 (Å)	C_2 (Å)	A_2 (Å)	σ_{D2}	σ_{C2}	σ_{A2}	N_1	N_2	Φ (%)	b_{n1}	b_{n2}
HEX	222	71	151	0.37	0.49	0.49	95	30	65	0.37	0.48	0.48	2	48	32	1.61	0.67
PEN	248	81	167	0.33	0.45	0.45	108	35	73	0.33	0.41	0.41	2	48	36	1.97	0.32
BUT	220	72	148	0.32	0.43	0.43	107	35	72	0.01	0.02	0.02	2	48	33	0.28	0.14

one of which had a high N (Table IV), because this allowed a better fit in a wide range of s values (toward a small s value).

Actually, as is shown in the TEM results [Fig. 4(b)], there was still good regularity in lamellar morphology, even if it was not as good as in the HOM sample, and the presence of almost linear lamellae organized into long stacks and of distorted and shorter lamellae. This could be related to the two populations, the first one made of lamellar stacks with high N and the second one related to the region of higher morphological disorder; here, blocks should have probably been present with a high value of C and A but should not have been organized into long stacks. The extension of the fit toward small s values could be related to the higher sensibility to the distortions in the region of s next to the zero-order maximum (see theoretical calculations).

Considerations of the same kind were even more relevant for the PEN and BUT samples. We employed the same model to obtain a good improvement of the fit in comparison with our calculations without lamellar distortions.

A very good fit was obtained for PEN (Fig. 7, R_{WP} = 1.5%) and especially for the BUT sample (Fig. 8, R_{WP} = 1.0%), that is, the more defective sample as concerns the lamellar morphology. Figure 8 shows the two populations leading to the best fit for the BUT sample.

As shown in Table IV, the lamellar thickness (C_1) was higher for PEN than for BUT; this was in agreement with our consideration of the TEM images.

Regarding the WAXS results, it was possible to compare (Table II) the Φ_{WAXS} and the crystallinity values determined SAXS (Φ_{SAXS}) and to note that Φ_{SAXS} was lower than Φ_{WAXS} but only for the three copolymer samples. This was probably because their morphology was not completely organized on stacks. As a matter of fact, the SAXS technique allowed us to determine only the Φ inside the lamellar stacks; on the contrary, the WAXS technique allowed us to evaluate the overall Φ of the sample. Then, the disordered regions outside the lamellar stacks were not part of the Φ_{SAXS}.

Instead, for the HOM sample, whose lamellar organization on stacks was excellent, we evaluated a Φ_{SAXS} higher than Φ_{WAXS} because outside the lamellar stacks, only a few amorphous regions were probably present.

CONCLUSIONS

The introduction of distortions of the second kind into the model describing the lamellar morphology of a polymer sample allowed for better results in the calculations of simulated SAXS profiles, and this was helpful in understanding morphology of polymer samples.

Our hypothesis was supported by TEM and WAXS results.

The homopolymer sample showed the presence of an excellent lamellar morphology; this was evident in the TEM image [Fig. 4(a)] and in the comparison of Φ_{WAXS} and Φ_{SAXS}.

In agreement with this, the theoretical model leading to the best fit was the variable lamellar stack model without distortions and with a single population representing the whole sample.

The situation was different for the three copolymer samples; with the increase in the lamellar distortions, evident in the TEM images [Fig. 4(b–d)], there was a higher correspondence with the model including second-kind distortions. This model allowed us to fit profiles even at small s value; furthermore, there was the presence of two lamellar populations, one leading to distorted lamellar stacks with $N \rightarrow \infty$ and the second probably leading to the blocks of crystalline and amorphous regions not organized on long stacks.

References

1. Blundell, D. J. Polymer 1978, 19, 1258.
2. Marega, C.; Marigo, A.; Cingano, G.; Zannetti, R.; Paganetto, G. Polymer 1996, 37, 5549.
3. Marigo, A.; Marega, C.; Zannetti, R.; Ajroldi, G.; Staccione, A. Macromolecules 1997, 30, 7862.
4. Marega, C.; Marigo, A.; Saini, R.; Ferrari, P. Polym Int 2001, 50, 442.
5. Vonk, C. G. J Appl Cryst 1978, 11, 541.
6. Sasanuma, Y.; Abe, A.; Sasanuma, T.; Kitano, Y.; Ishitani, A. J Polym Sci Part B: Polym Phys 1993, 31, 1179.
7. Marigo, A.; Marega, C.; Zannetti, R.; Sgarzi, P. Eur Polym J 1998, 34, 597.
8. Hindeleh, A. M.; Johnson, D. J. J Phys D 1971, 4, 259.
9. Vonk, C. G.; Pijpers, A. P. J Polym Sci Part B: Polym Phys 1985, 23, 2517.
10. Vonk, C. G. J Appl Crystallogr 1973, 6, 81.
11. Vonk, C. G. J Appl Crystallogr 1971, 4, 340.
12. James, F.; Roos, M. Comput Phys Commun 1975, 10, 343.
13. Young, R. A.; Prince, E. J Appl Crystallogr 1982, 15, 357.